Determination of the elemental distribution and chemical speciation in highly heterogeneous cementitious materials using synchrotron-based micro-spectroscopic techniques

M. Vespa [a,b,*,1], E. Wieland [a], R. Dähn [a], D. Grolimund [a], A.M. Scheidegger [a,b]

[a] Paul Scherrer Institute, Laboratory for Waste Management, 5232 Villigen PSI, Switzerland
[b] Department of Environmental Sciences, Swiss Federal Institute of Technology (ETH), Zürich, Switzerland

Abstract

Synchrotron-based micro-X-ray fluorescence (XRF) combined with scanning electron microscopy-based energy dispersive micro-analysis (EDS) has been used to determine the elemental distribution of contaminants (e.g., Ni) and of chemical elements inherent to the cement matrix (e.g., Si, Ca, Al, S) in hardened cement paste. Detailed information on the cement microstructure was gained by using backscattered electron (BSE) imaging. The results obtained from the complementary use of micro-XRF, EDS and BSE reveal that Ni is primarily distributed around inner calcium silicate hydrates (inner-C-S-H) and that Ni is preferentially associated with Al. This suggests the formation of a Ni–Al phase and its direct association with inner-C-S-H. Further information on the chemical speciation of Ni in relation to Al and S was obtained at selected regions of interests in the cement matrix using synchrotron-based micro-X-ray absorption spectroscopy (XAS). Data analysis shows that Ni is predominantly immobilized in layered double hydroxides, while predominant formation of ettringite was indicated from the Al and S XAS data.

The present study demonstrates that the combined use of micro-XRF, BSE, EDS and micro-XAS, opens up a powerful analytical approach to determine the distribution and the speciation of chemical elements in complex heterogeneous cementitious materials on the same region of interest with micro-scale resolution.

© 2007 Elsevier Ltd. All rights reserved.

Keywords: Synchrotron-based micro-XRF; micro-XAS; SEM-based BSE; SEM-based EDS; Cement

1. Introduction

Cement-based materials are commonly used in multi-barrier concepts developed worldwide for the safe disposal of hazardous and radioactive waste [e.g., 1,2]. In the case of the latter waste form, cement is used to condition and stabilize the waste materials and to construct the engineered barrier systems (container, backfill and liner materials) of repositories for radioactive waste. Thus, hardened cement paste (HCP) is an important component of the engineered barrier and plays an important role in the immobilization of waste ions in the cementitious near field of a repository. The immobilization potential of HCP originates from the selective binding properties for different chemical elements [e.g., 3], indicating that retention in cement systems is highly specific with respect to the mineral components and processes involved [e.g., 4–7]. HCP is composed of a very heterogeneous mineral assemblage with discrete particles in the nano- to micrometer size range. Therefore, any further attempt to link the immobilization of selected elements with the inherent heterogeneity of the cement matrix requires techniques well suited to address the appropriate length scale. Neglecting the micro-heterogeneity of such a complex matrix could result in misleading interpretations of immobilization mechanisms deduced from macroscopic studies, e.g., wet chemistry experiments. Thus, it is thought that spatially-resolved elemental, chemical and structural information could

* Corresponding author. Department of Environmental Sciences, Swiss Federal Institute of Technology (ETH), Zürich, Switzerland. Tel.: +41 56 310 2966; fax: +41 56 310 4595.

E-mail address: vespam@obs.ujf-grenoble.fr (M. Vespa).

[1] Current address. Environmental Geochemistry Group L.G.I.T. — Maison des Géosciences Université J. Fourier B.P. 53, 38041 Grenoble Cedex 9, France. Tel.: +33 4 76 828016.

often be the crucial key to decipher binding mechanisms in the cement matrix and offer novel insights into the chemical reactivity of cementitious systems.

Highly heterogeneous cementitious materials can be analyzed by a variety of analytical techniques, such as X-ray diffraction (XRD), transmission electron microscopy (TEM) and scanning electron microscopy (SEM). These methods are well suited to identify different mineral phases and to gain spatially-resolved information on the mineralogical composition, the morphology of the cementitious material and elemental distributions. For example, SEM provides spatially-resolved information on the microstructure and phase association as well as semi-quantitative information on the chemical composition of the different mineral phases by using a combination of backscattered electron (BSE) imaging with energy dispersive micro-analysis (EDS) [e.g., 8–11]. SEM-based BSE and EDS have proven to be suitable tools for investigating the microstructure of cement, the spatial distribution and the correlations among elements present in the cement matrix [e.g., 10,12]. Nevertheless, the main drawback of the above techniques is that they cannot provide information on the chemical speciation.

Only few analytical techniques allow the chemical speciation of elements in heterogeneous materials to be determined on the micro-scale. Synchrotron-based Fourier-transformed-infrared (FTIR)-spectro-microscopy and laser Raman microanalysis (LRMA) offer molecular information with a spatial resolution below 10 μm. However, the sensitivity of the above techniques is limited. Electron beam-based techniques, on the other hand, provide the best spatial resolution (nanometer range) that is presently achievable. For example, electron energy loss spectroscopy (EELS) allows the investigation of the chemical speciation of an element on a sub-micrometer-scale (e.g., redox state in a given matrix) based on the fine structure in the energy-loss spectrum [13]. Nevertheless, laborious sample preparation, sample exposure to ultra-high vacuum and possible radiation damages, especially in the case of cementitious materials, can limit its application [14].

The most promising technique for investigating the chemical speciation of elements in heterogeneous cementitious materials is synchrotron-based X-ray absorption spectroscopy (XAS). The method allows the speciation of chemical entities in complex matrices to be determined, even at low concentrations (concentration of X-ray absorber down to a few tens of ppm). Unknown species can be identified as precipitates in crystalline as well as in amorphous chemical environments, as surface-sorbed species or even in solution. XAS is a local probing technique which provides information on the coordination environment of an X-ray absorbing atom of interest within a distance up to ∼5 Å. Most frequently used XAS techniques are: X-ray absorption near edge structure (XANES) and extended X-ray absorption fine structure (EXAFS) [e.g., 15]. XANES is mainly used to discern the oxidation state of the X-ray absorber, based on the edge position, and for fingerprinting by comparing experimental spectra of unknown species with reference compounds. EXAFS, on the other hand, is employed to determine the coordination sphere of the X-ray absorber, i.e.,

type of neighboring atoms, bond length and coordination number [15–18].

In general, XAS does not yield spatially-resolved structural data, since the dimension of the X-ray beam is at most beamlines $>100 \times 100$ μm². In the past, much of the understanding of the coordination environment of contaminants bound in cementitious materials has been obtained by applying XAS on powder materials (bulk-XAS) [e.g., 4–7,19–22]. The studies focused on the use of bulk-XAS to determine the coordination environment of the element of interest in the bulk matrix. Furthermore, an increasing number of bulk-XAS studies have been carried out at the Ca and Al K-edge to examine the structure of hydrating calcium aluminates and poorly crystallized calcium-silicate-hydrate phases (C-S-H) [e.g., 23–26]. In bulk-XAS measurements the chemical speciation of an X-ray absorber of interest is determined by the averaged XAS signal generated from all individual species within the matrix of the investigated element (area typically probed ∼0.5 mm × 7 mm). In many cases, bulk-XAS is entirely sufficient to answer pertinent questions regarding the coordination environment of the element of interest in complex matrices, but the approach breaks down when mechanisms operative on the micro-scale have larger consequences on the chemical speciation. In particular, cementitious materials exhibiting micro-structural heterogeneities may provide different chemical environments within the matrix. Thus, it has been realized in the past years that solutions for large scale problems, such as metal contaminants in the environment, remediation and the storage of radioactive waste, should also be based on detailed information on the micro-scale. In view of the importance of small-scale processes and molecular-level mechanisms in complex heterogeneous systems, there has been a considerable effort to develop high resolution analytical synchrotron-based X-ray probes with which the wealth of structural information provided by XAS can be obtained on the micro-scale [27–38]. A key advantage of synchrotron-based X-ray analytical facilities is the combination of high photon flux, high brilliance and high wavelength tuneability with focused micro-beams. For in-depth reviews on micro-probe beamlines and applications of micro-spectroscopy on non-cementitious materials the reader is referred to Bertsch and Hunter [39], Manceau et al. [40] and Sutton et al. [41]. For micro-scale studies on cementitious materials the reader is referred to more recent publications [42–44].

In the present paper, a few case studies will be presented with the aim of illustrating the potential of the combined use of SEM-based BSE imaging and EDS micro-analyses with synchrotron-based micro-X-ray fluorescence (XRF) and micro-XAS. Micro-XRF is essential, in a first stage, to map the distribution of the chemical elements in the cement matrix. Subsequently, micro-XAS opens up the possibility of identifying the coordination environment of the element of interest on the molecular level. This multi-technique approach together with several methods of data analysis will be demonstrated using examples of the determination of the speciation of Ni, Al and S within a Ni enriched cement matrix and of Cr in a Cr rich cement matrix. The examples will be illustrated on the same region of interest in

the given sample. In the ideal case, the approach could even be applied on the same micron spot size.

2. Experimental

2.1. Sample preparation

The cement samples were prepared from a commercial sulfate-resisting Portland cement (CEM I 52.5 N HTS, Lafarge, France). Metal-enriched hydrated cement pastes were prepared by mixing a $Ni(NO_3)_2$ or K_2CrO_4 solution with unhydrated cement. The metal salts were dissolved in deionized water to obtain stock solutions with concentrations of 0.3 mol/L (pH ~ 4.5 and ~ 3). The solutions were mixed with the unhydrated cement at a water/cement (w/c) ratio of 0.4 according to the European Norm EN-196-3. The final metal concentrations of Ni(II) and Cr(VI) in the pastes were 5000 mg/kg. The cement pastes were filled into Plexiglas moulds, which were closed with a polyethylene lid, and hydrated for 30 days. The samples were stored in closed containers at 100% relative humidity. The cylinders were cut into several slices of ~ 1 cm thickness and dried in the glovebox (dry N_2 atmosphere, CO_2 and $O_2 < 2$ ppm, $T = 20 \pm 3$ °C). Some slices were crushed to obtain size fractions < 100 μm using a tungsten/carbide pebble mill. For bulk-XAS measurements the powder material was filled into Plexiglas holders and sealed with Kapton tape. Other slices were impregnated and polished for the preparation of thin sections. The polished thin sections, prepared by Spectrum Petrographics, Inc. (USA), were employed for both SEM-based BSE/EDS investigations and synchrotron-based micro-focused XRF/XAS measurements.

2.2. Scanning electron microscopy

The SEM investigations were conducted at the Laboratory for Construction Materials (IMX), Ecole Polytechnique Fédéral de Lausanne (EPFL) using a FEI Quanta 200 microscope. The FEI microscope was operated at an accelerating voltage of 15 kV and a beam current of 100 μA. The FEI microscope is equipped with a solid state detector for BSE imaging and with a Si(Li) detector for EDS analysis. The sample volume probed was ~ 1 μm^3.

2.3. Synchrotron-based investigations

2.3.1. Micro-XRF and micro-XAS data collection

Micro-XRF maps are based on the fluorescence signal detected from the sample under investigation. Elemental maps are generated by scanning the sample under the X-ray beam at a selected energy and correspond to qualitative elemental distribution. The proper choice of the beamline used for micro-focused investigations is crucial. Every beamline has an optimized (excitation) energy range, which depends, among others, on the X-ray source (e.g., bending magnet, insertion device), the crystals of the monochromator and the X-ray absorbing materials in the beam path (e.g., X-ray windows). Furthermore, micro-beam facilities offer specific experimental

setups, allowing experiments to be either conducted in air or in vacuum.

For the present study, micro-XRF maps of Ca, Si, Al and S were performed on the LUCIA beamline at the Swiss Light Source (SLS), Switzerland [35,36]. The micro-XRF maps were obtained by scanning the sample in a tender vacuum under the monochromatic beam with a beam size of 10×10 μm^2. For Ca, Si and Al the micro-XRF maps were recorded at the energy of 4.1 keV. For the S map the beam energy was set to 3.9 keV (below the Ca K-edge) in order to avoid saturation of the fluorescence detector by the Ca signal. The fluorescence signal was detected using a single element silicon drift diode. The micro-XRF map of Ni was collected at the Advanced Light Source (ALS) on beamline 10.3.2 in Berkeley, USA [37]. The micro-XRF map was obtained at the energy of 10 keV with a beam size of 5×5 μm^2 using a 7 element Ge-solid state detector and was carried out in air at room temperature.

Micro-XAS spectra at the K-edge of Ni (8.333 keV) and Cr (5.989 keV) were collected on beamline 10.3.2 (ALS) with a Si (111) crystal monochromator. The XAS spectra of Cr(III) and Cr(VI) reference solutions ($Cr(NO_3)_3$ and K_2CrO_4 solutions) were also collected on beamline 10.3.2 (ALS). The bulk-XAS spectra of Ni reference compounds were collected on the Swiss Norwegian Beam Line (SNBL) at the European Synchrotron Radiation Facility (ESRF) in Grenoble, France.

Micro-XAS spectra at the Al K-edge (1.559 keV) and S K-edge (2.470 keV) were recorded on the LUCIA beamline (SLS). The Al K-edge measurements were performed with a YB$_{66}$ (yttrium 66 boride crystal), whereas for the S K-edge measurements a Si(111) crystal monochromator was applied [35,36]. The beam size used was 10×10 μm^2. The XAS spectra of several reference compounds, i.e. ettringite ($Ca_6Al_2(SO_4)_3$ $(OH)_{12} \cdot 26H_2O$) [45], anhydrite ($CaSO_4$), Ca-monosulfoaluminate ($3CaO \cdot Al_2O_3 \cdot CaSO_4 \cdot 12H_2O$), Ca-monocarboaluminate ($3CaO \cdot Al_2O_3$ $CaCO_3 \cdot 11H_2O$), aluminate (C_3A, $Ca_3Al_2O_6$) and tetra calcium aluminate hydrated (C_4AH_{13}, $4CaO \cdot Al_2O_3$ $13H_2O$) [the latter four compounds from 46] were collected during the same measuring campaign and used to identify the Al and S speciation in the cement matrix. It should be noted that measurements of reference compounds are essential to identify the species in the cement matrix.

2.3.2. Micro-XAS data reduction

Data reduction was performed using the WinXAS 3.1 software package [e.g., 47]. All spectra were normalized by fitting a first-degree polynomial to the pre-edge and a third-degree polynomial to the post-edge regions. The Ni EXAFS spectra (k^3-weighted $\chi(k)$ functions) were generated by converting the energy to photoelectron wave vector units (Å^{-1}) using the origin E_0 of the first inflection point of the absorption edge. Radial Structure Functions were obtained by Fourier transforming the k^3-weighted $\chi(k)$ functions between 3.2 and 10.9 Å^{-1} using a Bessel window function with a smoothing parameter of 4. Multi-shell fits were performed in real space across the range of the first two shells ($\Delta R = 0.8$–3.5 Å). Theoretical phase and amplitude functions for the fit were calculated using FEFF 8.20 [48] and the structure of

Table 1
Structural information obtained from selected micro-EXAFS Ni K-edge data analysis together with reference compounds (spot 3 is indicated in Fig. 2)

Samples	Ni–O			Ni–Ni			Ni–Si			ΔE_0 (eV)	% Res
	CN	R (Å)	σ^2 (Å²)	CN	R (Å)	σ^2 (Å²)	CN	R (Å)	σ^2 (Å²)		
References											
Ni-phyllosilicate[a]	5.1	2.04	0.006	3.5	3.07	0.008[c]	3.7	3.26[Si]	0.008[c]	0.3	3.0
β-Ni(OH)$_2$	5.6	2.06	0.005	5.6	3.13	0.005[d]				−0.6	3.0
α-Ni(OH)$_2$	5.2	2.03	0.005	4.9	3.09	0.005[d]				3.0	4.4
Ni–Al LDH (LDH)	6.0	2.05	0.006	2.5	3.06	0.005[d]				1.1	4.5
Neo-formed Ni–Al LDH[b] (N-LDH)	5.7	2.04	0.004	3.9	3.07	0.005[d]				0.3	3.8
Cement sample											
spot 3	5.7	2.04	0.006	2.5	3.09	0.005[d]			−1.9	6.1

[a] Dähn et al.[62], [b] Scheidegger et al.[51], [c] correlated parameters and [d] fix parameters during fitting procedures.

R, CN, σ^2, and ΔE_0 stand for interatomic distances, coordination numbers, Debye–Waller factors and inner potential corrections.

Estimated error: $R_{(Ni–O)} \pm 0.02$ Å, $CN_{(Ni–O)} \pm 20\%$, $R_{(Ni–Ni)} \pm 0.02$ Å, $CN_{(Ni–Ni)} \pm 20\%$.

% Res: deviation between experimental data and fit given by the relative residual in percent.

N = number of data points, y_{exp} and y_{theo}: experimental and theoretical data points, respectively.

$$\%\text{Res} = \frac{\sum_{i=1}^{N} |y_{exp}(i) - y_{theo}(i)|}{\sum_{i=1}^{N} y_{exp}(i)} * 100$$

β-Ni(OH)$_2$. The amplitude reduction factor (S_0^2) was determined to be 0.85 [4]. Errors on the structural parameters were estimated from the analysis of a series of Ni reference compounds (see Table 1).

3. Results and discussion

3.1. Microscopic investigation

Fig. 1 shows results from the SEM-BSE/EDS investigations on the Ni enriched HCP. The aim of the microscopic investigations was to discern the spatial distribution of the cement-derived elements Ca, Si, Al, S, Fe and of Ni in order to elucidate possible association of Ni with specific minerals of the cement matrix. The EDS maps of Ca, Si and Fe are shown elsewhere [43] since no substantial information could be extracted in connection with the present study. The S EDS map reveals a relative homogeneous distribution, whereas the Al map illustrates highly enriched regions. Furthermore, the SEM–EDS map of Ni shows a heterogeneous distribution in the cement matrix. In particular, Ni appears to be enriched in bright rims around inner-C-S-H phases. A weak correlation, observed between Ni and Al at these rims, could be substantiated by EDS-point analyses [43]. The EDS-point analyses further revealed that this Ni-rich phase has a variable Ni content, ranging from ∼5 weight% (wt.%) up to ∼10 wt.%. The information gained from the SEM-BSE/EDS investigations allowed to propose a reaction scheme for Ni immobilization in the hydrating cement [43]. During hydration the major clinker mineral alite, which decomposes faster than belite, acts as a highly reactive zone for the formation of both inner-C-S-H and the newly-formed Ni phase. Outer-C-S-H, on the other hand, fills the porous space, and is generally finely intermixed with portlandite and several other minor hydrated phases, such as

ettringite, Ca-monosulfoaluminate, Ca-monocarboaluminate, tetra calcium aluminate hydrate, and hydrotalcite-like phases (hydrotalcite: $Mg_4Al_2(OH)_{12} \cdot CO_3 \cdot 2H_2O$) [49,50]. The key information obtained from SEM-EDS investigations is that the Ni-rich rims form around inner-C-S-H, the hydration product of alite, indicating preferential accumulation of Ni in these highly reactive zones. Correlation with Al, in these zones, further suggests that a mixed Ni–Al phase could form. Nevertheless, it clearly appears that SEM-based BSE and EDS do not provide any further details on the chemical speciation of Ni or Al in these mixed phases.
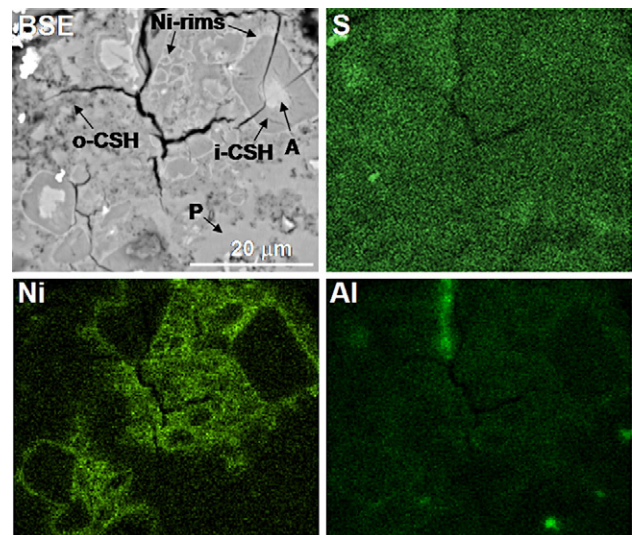

Fig. 1. BSE image of a Ni-rich region together with EDS elemental distribution maps of Ni, Al and S. Notations: A = alite, P = portlandite (Ca(OH)$_2$), i-CSH = inner-C-S-H, o-CHS = outer-C-S-H.
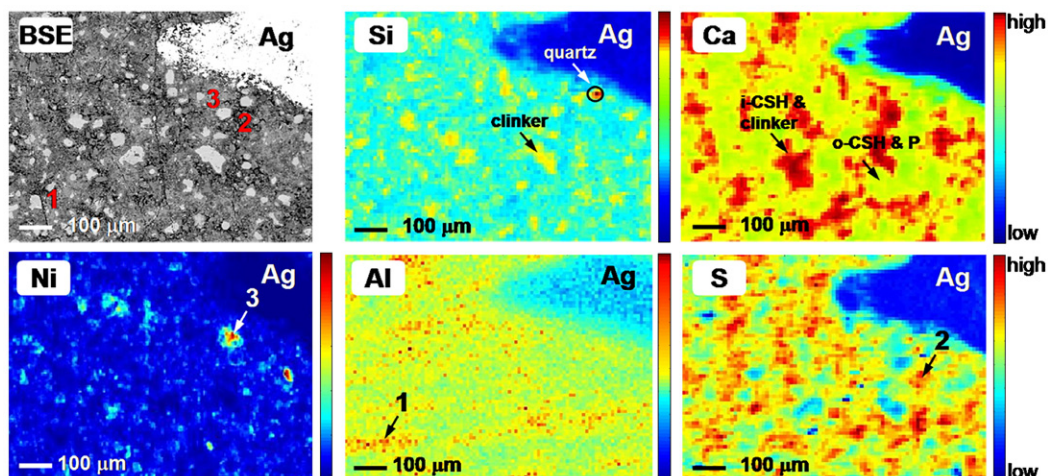
Fig. 2. BSE image and micro-XRF elemental distribution maps of Si, Ca, Ni, Al and S in a ∼700×1000 μm overview of a Ni enriched hydrated cement matrix. The region marked with '3' corresponds to the same region illustrated in Fig. 1. Micro-XAS selected regions for Al K-edge (1), S K-edge (2) and Ni K-edge (3) measurements are marked with numbers on the BSE image and the respective elemental maps. Ag = silver spot used as marker, i-CSH = inner-C-S-H, o-CHS = outer-C-S-H, P = portlandite (Ca(OH)$_2$).

3.2. Synchrotron-based investigations

3.2.1. Micro-XRF investigations

Micro-XRF elemental maps are required in a first step of synchrotron-based speciation studies to gain an overview on the distribution of the investigated chemical elements. In this study, Al, S and Ni maps were determined, among others [43], to localize enriched spots of these elements in the cement matrix. At these selected spots, speciation studies were carried out using the micro-XAS technique. In the ideal case, it is desirable to investigate the same areas of interests or spots, respectively, previously studied by SEM-based BSE and EDS. To achieve this objective, a silver spot, used as a marker, was implemented to identify the area of interest for both microscopic and micro-spectroscopic investigations (Fig. 2, marked with 'Ag').

Micro-XRF maps of ∼700×1000 μm (Fig. 2) were recorded in the same area previously imaged by SEM (Fig. 1). The BSE image shown in Fig. 2 reveals bright grains (clinker minerals), fine darker grains (hydrated minerals), and black zones, which correspond to the pore space in the hydrated cement matrix [43]. The region investigated by SEM is strongly hydrated, lies between two clinker minerals and is marked with number '3' on the BSE image in Fig. 2. Micro-XRF mapping focused on the elemental distribution of Si, Ca, Ni, Al and S. The Si map allows clinker minerals to be identified (high concentrated regions). The highest concentrated Si region (circled area) is a quartz grain. The latter finding was confirmed by BSE imaging (details with high magnification are not shown). The Ca distribution mainly reflects zones of unhydrated clinker and hydrated cement minerals. The high concentrated Ca regions indicate the presence of mainly inner-C-S-H and clinker minerals. Regions with less Ca indicate the formation of outer-C-S-H and portlandite. Knowledge of the S distribution in combination with the Al map allows regions of high Al and high S concentrations to be distinguished from regions with high Al concentrations and low or no S contents. The latter case

indicates the presence of non-hydrated and/or hydrated aluminates such as Ca-monocarboaluminate, whereas areas with high Al and S concentrations indicate the presence of ettringite and/or Ca-monosulfoaluminate [50]. The combination of Ni and Al distribution maps is needed to localize the area of interest for chemical speciation studies on Ni by using the micro-XAS technique. Note that mixed Ni–Al phases are expected to form [43]. With the above given information, the region of interest (spot 3) for the Ni speciation study can be easily retrieved.

It should be noted that the fluorescence signals detected by SEM-EDS and by synchrotron-based micro-XRF measurements are distinct, due to differences in the penetration depths. For example, spot-like structures, instead of rims, appear on the micro-XRF map of Ni (Fig. 2) due to the higher penetration depth (e.g., ∼150 μm at ∼8 keV for C-S-H phases) and the lower spatial resolution (few micron) of the X-rays compared to those of the electrons (penetration depth ∼1 μm; spatial resolution in the nanometer range) [43]. Nevertheless, in spite of the different patterns appearing on the SEM and micro-XRF images, it is possible to unequivocally identify the area of interest based on the position of the silver marker and the Ca and Si distribution maps determined by the two techniques.

3.2.2. Micro-XAS investigations

In the following section, a stepwise approach of data analysis and treatment will be outlined to illustrate the possibilities of retrieving the chemical information available from the XANES and EXAFS data. Comparison of the experimental spectra in their normalized form, the corresponding k^3-weighted $\chi(k)$ functions and the Fourier transform (FT) with those of reference compounds gives first indications of the kind of coordination environment of the unknown species under investigation.

All spots selected for micro-XAS investigations reveal high concentrations of the respective elements (Fig. 2). The spectra, presented in this section, were collected at spot 1 in the case of

Al, at spot 2 in the case of S and at spot 3 in the case of Ni (Fig. 2). Note that the Ni spot 3, outlined in Fig. 2, was analyzed by SEM, micro-XRF and micro-XAS and corresponds to the area displayed in Fig. 1.

Fig. 3 shows Al and S spectra, collected in the XANES region. At the Al K-edge (1559 eV) the measurement was conducted over a limited experimental energy range due to the overlap with Si. Note that the Si K-edge at 1839 eV is only 280 eV above the Al K-edge. In the case of S, only micro-XANES data were collected due to the difficult background of S within the cement matrix. The micro-XANES spectrum of spot 1, at the Al K-edge (Fig. 3a), reveals strong similarities with that of ettringite ($Ca_6Al_2(SO_4)_3(OH)_{12} \cdot 26H_2O$). In particular, the positions of the absorption edge and the spectral feature 'A' are well reproduced in both spectra. This observation indicates that ettringite could be the main Al-forming phase at this particular spot.

In the case of S, similarities between the spectrum of spot 2 with the reference compound ettringite are also observed. Furthermore, the micro-XANES spectrum of $Ca(SO)_4$ shows two features, 'B' and 'C', which are neither present in the reference compounds of ettringite and Ca-monosulfoaluminate nor in the selected spot 2 (Fig. 3b). Moreover, the maximum of feature 'D', observed for spot 2 and comparable to the same feature in ettringite, is slightly shifted to higher energy compared to Ca-monosulfoaluminate. Thus, these findings suggest that, at this particular spot, ettringite is the predominant species forming.

Fig. 4 shows the data from micro-EXAFS measurement at the Ni spot and relevant Ni reference compounds. Fig. 4a shows the k^3-weighted micro-EXAFS spectra, whereas the corresponding Fourier transforms (FT) are displayed in Fig. 4b. The experimental Ni EXAFS spectrum collected at spot 3 shows a broad oscillation at ~ 4 Å^{-1}, which is located at a k-range that agrees with the position of the first major oscillation observed in the spectrum of a neo-formed LDH phase (N-LDH) [51] (Fig. 4a). Furthermore, the

splitting of the oscillation at ~ 8 Å^{-1} is a characteristic beat pattern. Scheinost and Sparks demonstrated that this beat pattern indicates the presence of Ni–Al LDH, and can be used as a fingerprint [52]. In fact, the beat pattern at ~ 8 Å^{-1} is observed in both Ni–Al LDH spectra (LDH and N-LDH), whereas the other reference compounds (α-Ni(OH)$_2$, β-Ni(OH)$_2$ and Ni-phyllosilicate) show an elongated upward oscillation ending in a sharp tip at ~ 8.5 Å^{-1}. Thus, the presence of the beat pattern at ~ 8 Å^{-1} together with the observed spectral features at ~ 4 Å^{-1} suggests that a Ni–Al LDH phase has formed at Ni-rich spot 3. The corresponding FT (Fig. 4b) shows that the positions of the first and second FT peaks, as well as the shape of the imaginary part of the Ni spot do agree well with those from Ni–Al LDH compounds. Note that the amplitude of the second peak in the experimental spectrum is clearly reduced compared to the Ni-hydroxide reference spectra. Such an amplitude reduction results from the destructive interference of Ni and Al backscattering contribution [4,5,52, see below].

The above observations suggest the predominant formation of a single species for all investigated elements. Nevertheless, it should be considered that mixtures of different species could contribute to the micro-XANES or micro-EXAFS spectra, causing an averaged signal. This is due to the fact that the beam size ($\sim 5 \times 5$ μm^2) might be significantly larger than the expected size of the Al-, S- and Ni-containing phases formed in the cement matrix at the different spots. To identify the number of species probed, principal component analysis (PCA) may be applied. The success of this method depends on the existence of an extensive database of relevant reference spectra. If the database contains the references making up the experimental spectrum, PCA can be used to determine the number of species that are present. Subsequently, target transformation (TT) can be implemented to test which reference compound is necessary to reconstruct the experimental spectrum. For example, a combination of PCA and TT has been successfully applied to determine the chemical species
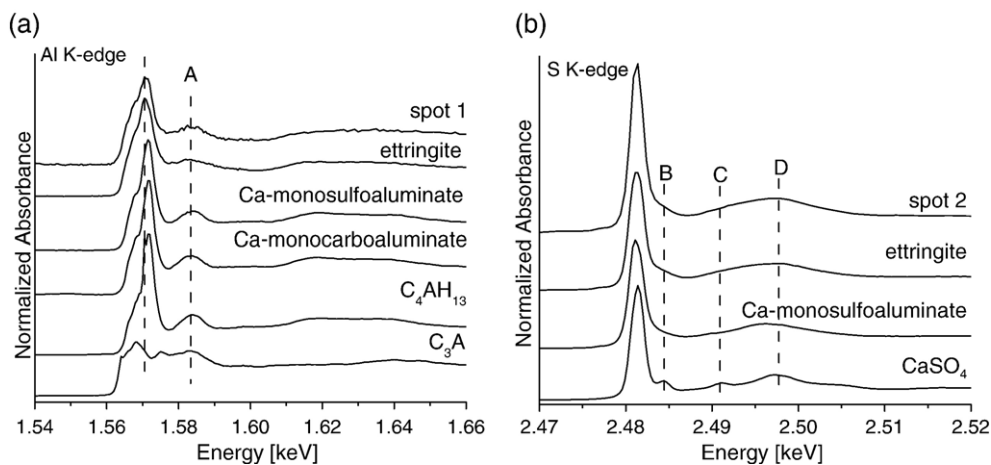

Fig. 3. a) Al K-edge micro-XANES experimental spectrum of hydrated cement and powder experimental spectra of several reference compounds: ettringite ($Ca_6Al_2(SO_4)_3(OH)_{12} \cdot 26H_2O$), Ca-monosulfoaluminate ($3CaO \cdot Al_2O_3 \cdot CaSO_4 \cdot 12H_2O$), Ca-monocarboaluminate ($3CaO \cdot Al_2O_3$ $CaCO_3 \cdot 11H_2O$), aluminate (C_3A, $Ca_3Al_2O_6$) and tetra calcium aluminate hydrate (C_4AH_{13}, $4CaO \cdot Al_2O_3$ $13H_2O$); b) S K-edge micro-XANES experimental spectrum of hydrated cement and powder experimental spectra of ettringite, Ca-monosulfoaluminate and Ca-sulfate reference compounds. The dashed lines indicate spectral features explained in detail in the text.
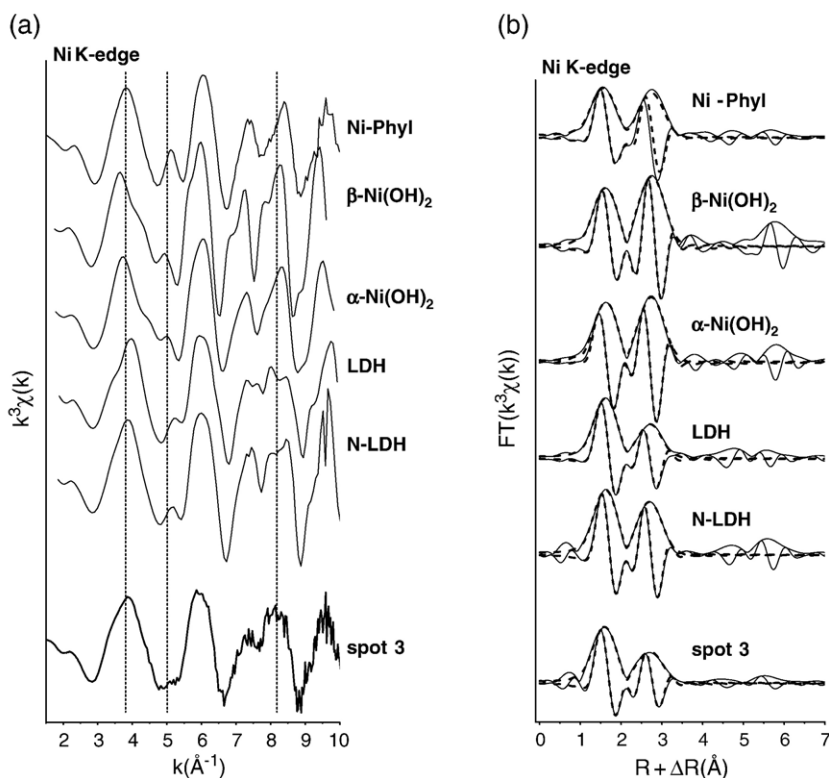
Fig. 4. Ni K-edge bulk-EXAFS experimental spectra of reference compounds and micro-EXAFS of a selected Ni-rich spot 3 (spot 3 is illustrated in Fig. 2); a) k^3-weighted, normalized, background-subtracted spectra; b) experimental (solid line) and theoretical (dashed line) Fourier transforms (modulus and imaginary parts) obtained from the spectra presented in a. Notations: N-LDH = neo-formed Ni–Al LDH [51], LDH = synthetic Ni–Al LDH (Ni:Al, 2:1) [61], Ni-Phyl = Ni-phyllosilicate [62].

present in complex natural systems [e.g., 40,53]. In the course of this study, PCA was tested for the investigated cement system, in particular to determine the number of species formed at the Ni spot. In the case of Ni, it was observed that PCA analysis gives no conclusive results, due to the strong similarity of the reference spectra (Fig. 4a). Thus, some assumptions concerning the chemical speciation had to be made, in order to further determine and quantify the amount of single species present at the investigated spot.

In order to achieve this goal, linear combination (LC) analysis was employed as the method of choice. In the case of Ni, it was assumed that Ni–Al LDH is intermixed with α- and β-Ni(OH)$_2$. Formation of the latter compounds is expected based on thermodynamic constraints, due to the high Ni concentrations of the solution used to start the hydration process [22]. In the case of Al, all possible Al-containing cement phases have been considered. Thus, LC fits for the experimental Al spectra were performed using the references shown in Fig. 3a. In the case of S, LC analysis was not possible, due to the extreme similarity of the reference XANES spectra, especially of ettringite and Ca-monosulfoaluminate.

Best LC fits for the Al spot 1 were obtained by combining ∼80% ettringite and ∼20% C$_3$A. Note that the predominant formation of ettringite is expected in the given cement matrix based on the study of Lothenbach and Wieland [50]. In the case of Ni spot 3, the LC analysis indicate that predominantly Ni–Al LDH has formed (∼70%) together with some β-Ni(OH)$_2$

(∼30%). Comparison of further LC analysis, previously carried out for Ni bulk-XAS measurements [22], with the data from this study indicate that the Ni species observed on the micro-scale are relevant for the whole cement matrix. This comparison between bulk- and micro-XAS results is compulsory to assess the relevance of the speciation determined on the micro-scale.

If good quality EXAFS spectra are available over an extended region above the absorption edge (from ∼50 eV to ∼1000 eV above the edge), structural parameters, such as coordination numbers (CN), bond distances (R) and system disorder (Debye–Waller), can be derived via a multi-shell fit analysis. The structural parameters derived from multi-shell analysis for the Ni K-edge EXAFS spectra derived from the FT ($\Delta R = 0.8$–3.5 Å) are summarized in Table 1. The first coordination shell was fitted with Ni–O backscattering pairs. The second coordination shell was fitted solely using Ni–Ni pairs, as the discrimination of Ni–Ni and Ni–Al backscattering pairs in Ni–Al LDH is problematic due to a phase interference [4,5, see below]. To be able to compare the coordination numbers of the Ni–Ni backscattering pairs (CN$_{Ni–Ni}$) determined for spot 3 and the references, the Debye–Waller factor was fixed to 0.005 Å^2 as determined for the β-Ni(OH)$_2$. The first FT peak corresponds to an octahedral coordination of Ni with ∼6 oxygen atoms at 2.04 Å (Table 1). The second FT peak reveals strongly reduced CN$_{Ni–Ni}$ (2.5) compared to α-Ni(OH)$_2$ (∼5) [54] and β-Ni(OH)$_2$ (∼6) [55]. Note that the CN$_{Ni–Ni}$ derived for the second shell is comparable to that determined
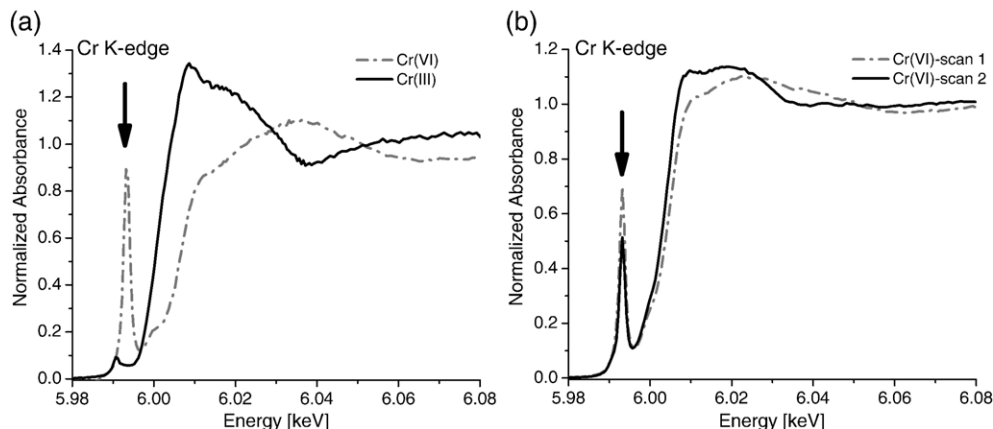
Fig. 5. Cr K-edge micro-XANES spectra; a) reference spectra of K_2CrO_4 and $Cr(NO_3)_3$ solutions used to identify Cr(VI) and Cr(III) species, respectively; b) experimental spectra obtained from a thin section of Cr(VI) enriched cement. The spectrum indicated with a dashed line is the first spectrum collected under the X-ray beam. The spectrum illustrated with a solid line was collected after ~20 min exposure time on the same spot. Arrows indicate pre-edge feature.

from the Ni–Al LDH spectrum. The reduced CN_{Ni-Ni} is due to Ni substitution by Al in Ni–Al LDH, which results in a significant destructive phase interference between Ni and Al EXAFS contributions [5]. Although the CN of the second shell (CN_{Ni-Ni}) agree very well with that of Ni–Al LDH, the overall Ni–Ni distance is longer (R_{Ni-Ni}=3.09 Å) at the Ni spot 3 than in Ni–Al LDH compounds (3.06–3.07 Å). Vespa et al. [22] attributed the longer R_{Ni-Ni} to the presence of β-Ni(OH)$_2$ impurities (R_{Ni-Ni}=3.13 Å). The findings from the detailed interpretation of the EXAFS spectra, thus, further substantiate the results from the LC analysis, which suggest the presence of a mixture of Ni–Al LDH and β-Ni(OH)$_2$.

3.2.3. XAS as a tool to differentiate oxidation states

The determination of the different oxidation states is an important issue in the case of redox-sensitive elements. For example, knowledge of the oxidation state of elements such as Tc [e.g., 19,56], Se, I [e.g., 6,21] and Co [e.g., 44] is of major importance in conjunction with the safe disposal of radioactive waste. In the cement research the determination of the oxidation state of Cr is particularly important. Cr, especially Cr(VI), is known as a skin sensitizer, which can lead to a frequent health disorder, 'dermatitis' [e.g., 57–59]. The most promising technique to determine oxidation states in complex matrices is XAS.

The identification of Cr(VI) and Cr(III) is based on the yield of the pre-edge feature in the XANES spectra (Fig. 5a). This feature is pronounced in the case of Cr(VI), but very small for Cr(III). The pre-edge feature is an electronic transition from a core level to the lowest unoccupied or partially occupied energy level. In the case of the K-edge of Cr(VI) the pre-edge feature is due to a 1s→3d transition [60]. Although identification of Cr(VI) and Cr(III) is straightforward, and has been successfully used in the past to differentiate Cr(III) and Cr(VI) in cementitious materials [e.g., 42], micro-XAS studies with Cr on cementitious materials have been proven to be problematic at synchrotrons of the new generation with highly focused and intense beams. During the micro-XAS measurements carried out at 10.3.2 (ALS) it was observed that the oxidation state of Cr(VI) changed under the micro-beam [beam size of 5×5 μm^2 and a photon flux of $\sim 1 \times 10^9$ ph/s/μm^2, 37]. In this study CrO_4^{2-} (Cr(VI)) was found to reduce to Cr(III) within ~20 min after irradiation by the X-ray beam. Fig. 5b shows the first scan of a Cr(VI) enriched hydrated cement matrix on a region of interest rich in Cr(VI). The second scan was collected after ~20 min exposure time, showing the reduction of Cr(VI) to Cr(III). The above investigations clearly demonstrated that, although XAS is considered to be a non-destructive technique, special care has to be taken to exclude artefacts caused by beam damage for sensitive redox systems. Neglecting such phenomena could lead to a misinterpretation of the XAS data and consequently give rise to conflicting information on the immobilization processes involved.

4. Conclusions

The multi-technique approach presented in this paper illustrates that, the combination of synchrotron-based micro-XRF and micro-XAS with electron microscopic investigations (BSE, EDS) allows in situ micro-scale speciation studies to be carried out on heterogeneous cementitious matrices. Each of the above presented techniques (micro-XRF, micro-XAS, BSE, EDS) has unique capabilities and, used in a complementary way, allows the elemental distribution and chemical speciation of the elements of interest to be determined on the same investigated area. Moreover, it can be expected that in the near future, further technical developments of high efficiency zones plates for excitation energies of 5–15 keV will allow decreasing the spatial resolution from the micro-scale to the nano-scale for chemical speciation studies. This step will enable to probe single species, and is, thus, considered to be an essential improvement for the investigation of cementitious systems, since most phases are nano-particles.

References

[1] M. Schmidt, P. Beckefeld, R. Götz, S. Kamsties, C. Kretz, N. Molitor, U. Neck, P. Vogel, Reststoff-und Abfallverfestigung, Immobilisierung von Schadstoffen-Recycling-Verbesserung der Deponiefähigkeit, Expert Verlag, Renningen-Malmheim, 1995.

[2] N. Chapman, C. McCombie, Principles and Standards for the Disposal of Long-Lived Radioactive Wastes, 1st ed.Elsevier Science, Ltd., Oxford, 2003.

[3] F.P. Glasser, Chemistry of cement-solidified waste forms, in: R.D. Spence (Ed.), Chemistry and Microstructure of Solidified Waste Forms, Lewis Publishers, Boca Raton, 1993, pp. 1–39.

[4] A.M. Scheidegger, E. Wieland, R. Dähn, P. Spieler, Spectroscopic evidence for the formation of layered Ni–Al double hydroxides in cement, Environmental Science and Technology 34 (2000) 4545–4548.

[5] A.M. Scheidegger, E. Wieland, A.C. Scheinost, R. Dähn, J. Tits, P. Spieler, Ni phases formed in cement and cement systems under highly alkaline conditions: an XAFS study, Journal of Synchrotron Radiation 8 (2001) 916–918.

[6] I. Bonhoure, A.M. Scheidegger, E. Wieland, R. Dähn, Iodine species uptake by cement and CSH studied by K-edge X-ray absorption spectroscopy, Radiochimica Acta 90 (2002) 647–651.

[7] I. Bonhoure, E. Wieland, A.M. Scheidegger, M. Ochs, D. Kunz, EXAFS study of Sn (IV) immobilization by hardened cement paste and calcium silicate hydrates, Environmental Science and Technology 37 (2003) 2184–2191.

[8] J.G. Catalano, J.P. McKinley, J.M. Zachara, S.M. Heald, S.C. Smith, G.E. Brown Jr., Changes in uranium speciation through a depth sequence of contaminated Hanford sediments, Environmental Science and Technology 40 (8) (2006) 2517–2524.

[9] C. Famy, K.L. Scrivener, A.K. Crumbie, What causes differences of C-S-H gel grey levels in backscattered electron images? Cement and Concrete Research 32 (9) (2002) 1465–1471.

[10] K.L. Scrivener, Backscatter electron imaging of cementitious microstructures: understanding and quantification, Cement and Concrete Composites 26 (2004) 935–945.

[11] T. Kirpichtchikova, A. Manceau, L. Spadini, F. Panfili, M. Marcus, T. Jacquet, Speciation and solubility of heavy metals in contaminated soil using X-ray microfluorescence, EXAFS spectroscopy, chemical extraction, and thermodynamic modelling, Geochimica et Cosmochimica Acta 70 (2006) 2163–2190.

[12] C. Famy, K.L. Scrivener, A. Atkinson, A.R. Brough, Effects of an early or a late heat treatment on the microstructure and composition of inner C-S-H products of Portland cement mortars, Cement and Concrete Research 32 (2) (2002) 269–278.

[13] R.F. Egerton, M. Malac, EELS in the TEM, Journal of Electron Spectroscopy and Related Phenomena 143 (2005) 43–50.

[14] R.F. Egerton, P. Li, M. Malac, Radiation damage in the TEM and SEM, Micron 35 (2004) 399–409.

[15] D.C. Koningsberger, R. Prins, X-ray Absorption, John Wiley & Sons, New York, 1987.

[16] G.E. Brown Jr., Spectroscopic studies of chemisorption reaction mechanisms at oxide–water interfaces, in: M.F. Hochella, A.F. White (Eds.), Mineral–Water Interface Geochemistry, The Mineralogical Society of America, Washington DC, 1990, pp. 309–353.

[17] L. Charlet, A. Manceau, Structure, formation, and reactivity of hydrous oxide particles: insights from X-ray absorption spectroscopy, in: P.J. Buffle, H.P. van Leeuwen (Eds.), Environmental Particles, Lewis Publishers, Boca Raton, 1993, pp. 117–164.

[18] P.A. Fenter, M.L. Rivers, N.C. Sturchio, S.R. Sutton, Applications of Synchrotron Radiation in Low-Temperature Geochemistry and Environmental Science, The Mineralogical Society of America, Washington DC, 2002.

[19] P.G. Allen, G.S. Siemering, D.K. Shuh, J.J. Bucher, N.M. Edelstein, C.A. Langton, Technetium speciation in cement waste forms determined by X-ray absorption fine structure spectroscopy, Radiochimica Acta 76 (1997) 77–86.

[20] P. Zhao, P.G. Allen, E.R. Sylvester, B.E. Viani, The partitioning of uranium and neptunium onto hydrothermally altered concrete, Radiochimica Acta 88 (2000) 729–736.

[21] I. Bonhoure, I. Baur, E. Wieland, C.A. Johnson, A.M. Scheidegger, Uptake of Se(IV/VI) oxyanions by hardened cement paste and cement minerals: an X-ray absorption spectroscopy study, Cement and Concrete Research 36 (2006) 91–98.

[22] M. Vespa, R. Dähn, D. Grolimund, E. Wieland, A.M. Scheidegger, Spectroscopic investigation of Ni speciation in hardened cement paste, Environmental Science and Technology 40 (2006) 2275–2282.

[23] N. Richard, N. Lequeux, P. Boch, An X-ray absorption study of phases formed in high-alumina cements, Advances in Cement Research 7 (28) (1995) 159–169.

[24] N. Lequeux, A. Moreau, S. Philippot, P. Boch, Extended X-ray absorption fine structure investigation of calcium silicate hydration, Journal of the American Ceramic Society 82–5 (1999) 1299–1306.

[25] R.J. Kirkpatrick, G.E. Brown, N. Xu, X. Cong, X-ray absorption spectroscopy of C-S-H and some model compounds, Advances in Cement Research 9 (33) (1997) 31–36.

[26] N. Richard, N. Lequeux, P. Florian, Changes in the structure of $CaAl_2O_{14}H_2O$ during heat treatments: an X-ray absorption spectroscopy and ^{27}Al NMR studies, in: P. Colombet, A.R. Grimmer, H. Zanni, P. Sozanni (Eds.), Nuclear Magnetic Resonance Spectroscopy of Cement-Based Materials, Springer-Verlag, Berlin, 1998, pp. 321–329.

[27] M.L. Rivers, S.R. Sutton, J.V. Smith, A synchrotron X-ray-fluorescence microprobe, Chemical Geology 70 (1988) 179.

[28] F. Vanlangevelde, G.H.J. Tros, D.K. Bowen, R.D. Vis, The synchrotron radiation microprobe at the SRS, Daresbury (UK) and its applications, Nuclear Instruments & Methods in Physics Research. Section B, Beam Interactions with Materials and Atoms 49 (1990) 544–550.

[29] R. Devoti, F. Zontone, C. Tuniz, F. Zanini, A synchrotron radiation microprobe for X-ray-fluorescence and microtomography at Elettra — focusing with bent crystals, Nuclear Instruments & Methods in Physics Research. Section B, Beam Interactions with Materials and Atoms 54 (1991) 424–428.

[30] K. Janssens, L. Vincze, F. Adams, K.W. Jones, Synchrotron radiation-induced X-ray-microanalysis, Analytica Chimica Acta 283 (1993) 98–110.

[31] S. Hayakawa, S. Goto, T. Shoji, E. Yamada, Y. Gohshi, X-ray microprobe system for XRF analysis and spectroscopy at SPring-8 BL39XU, Journal of Synchrotron Radiation 5 (1998) 1114–1116.

[32] M. Newville, S. Sutton, M. Rivers, P. Eng, Micro-beam X-ray absorption and fluorescence spectroscopies at GSECARS: APS beamline 131D, Journal of Synchrotron Radiation 6 (1999) 353–355.

[33] S. Bohic, A. Simionovici, A. Snigirev, R. Ortega, G. Deves, D. Heymann, C.G. Schroer, Synchrotron hard X-ray microprobe: fluorescence imaging of single cells, Applied Physical Letters 78 (2001) 3544–3546.

[34] A. Somogyi, M. Drakopoulos, L. Vincze, B. Vekemans, C. Camerani, K. Janssens, A. Snigirev, F. Adams, ID18F: a new micro-X ray fluorescence end-station at the European Synchrotron Radiation Facility (ESRF): preliminary results, X-ray Spectrometry 30 (2001) 242–252.

[35] M. Janousch, A.-M. Flank, P. Lagarde, G. Cauchon, S. Bac, J.M. Dubuisson, T. Schmidt, R. Wetter, D. Grolimund, A.M. Scheidegger, LUCIA — a new 1–7 keV μ-XAS beamline, AIP Conference Proceedings (2004) 312.

[36] P. Lagarde, A.-M. Flank, D. Vantelon, M. Janousch, Micro-soft X-ray spectroscopy with the LUCIA beamline, X-Ray Absorption Fine Structure-XAFS13, 2007, pp. 852–857.

[37] M. Marcus, A.A. MacDowell, R. Celestre, A. Manceau, T. Miller, H.A. Padmore, R.E. Sublett, Beamline 10.3.2 at ALS: a hard X-ray microprobe for environmental and material sciences, Journal of Synchrotron Radiation 11 (2004) 239–247.

[38] A.M. Scheidegger, D. Grolimund, M. Harfouche, M. Willimann, B. Meyer, R. Dähn, D. Gavillet, M. Nicolet, P. Heimgartner, The micro-XAS beamline at the Swiss Light source (SLS): a new analytical facility suited for X-ray micro-beam investigations with radioactive samples, Speciation Techniques and Facilities for Radioactive Materials at Synchrotron Light Sources, 2006, pp. 81–86.

[39] P.M. Bertsch, D.B. Hunter, Applications of synchrotron-based X-ray microprobes, Chemical Reviews 101 (6) (2001) 1809–1842.

[40] A. Manceau, M. Marcus, N. Tamura, Quantitative speciation of heavy metals in soils and sediments by synchrotron X-ray techniques, in: P.A. Fenter, M.L. Rivers, N.C. Sturchio, S.R. Sutton (Eds.), Application of Synchrotron Radiation in Low-Temperature Geochemistry and Environmental Science, Mineralogical Society of America, Washington, DC, 2002, pp. 341–428.

[41] S.R. Sutton, P.M. Bertsch, M. Newville, M. Rivers, A. Lanzirotti, Microfluorescence and microtomography analyses of heterogeneous earth and environmental materials, Applications of Synchrotron Radiation in Low-Temperature Geochemistry and Environmental Science, American Mineralogical Society, 2002, pp. 429–483.

[42] J. Rose, A. Bénard, J.S., D. Borschneck, J.-L. Hazemann, P. Cheylan, A. Vichot, J.-Y. Bottero, First insights of Cr speciation in leached Portland cement using X-ray spectromicroscopy, Environmental Science and Technology 37 (2003) 4864–4870.

[43] M. Vespa, R. Dähn, E. Gallucci, D. Grolimund, E. Wieland, A.M. Scheidegger, Micro-scale investigation of Ni uptake by cement using a combination of scanning electron microscopy and synchrotron-based techniques, Environmental Science and Technology 40 (2006) 7702–7709.

[44] M. Vespa, R. Dähn, D. Grolimund, E. Wieland, A.M. Scheidegger, Co speciation in hardened cement paste: a macro- and micro-spectroscopic investigation, Environmental Science and Technology 41 (2007) 1902–1908.

[45] M. Ochs, B. Lothenbach, E. Giffaut, Uptake of oxo-anions by cements through solid-solution formation: experimental evidence and modelling, Radiochimica Acta 90 (2002) 639–646.

[46] T. Matschei, B. Lothenbach, F.P. Glasser, The AFm-phase in Portland cement, Cement and Concrete Research 37 (2007) 118–130.

[47] T. Ressler, WinXAS: a program for X-ray absorption spectroscopy data analysis under MS-Windows, Journal of Synchrotron Radiation 5 (2) (1998) 118–122.

[48] J.J. Rehr, R.C. Albers, Theoretical approaches to X-ray absorption fine structure, Reviews of Modern Physics 72 (3) (2000) 621–653.

[49] B. Lothenbach, F. Winnefeld, Thermodynamic modelling of the hydration of Portland cement, Cement and Concrete Research 36 (2006) 209–226.

[50] B. Lothenbach, E. Wieland, A thermodynamic approach to the hydration of sulphate-resisting Portland cement, Waste Management 26 (2006) 706–719.

[51] A.M. Scheidegger, G.M. Lamble, D.L. Sparks, The kinetics of nickel sorption on phyrophyllite as monitored by X-ray absorption fine structure (XAFS) spectroscopy, Journal de Physique IV France 7 (C2) (1997) 773–775.

[52] A.C. Scheinost, D.L. Sparks, Formation of layered single- and double-metal hydroxide precipitates at the mineral/water interface: a multiple-scattering XAFS analysis, Journal of Colloid and Interface Science 223 (2000) 1–12.

[53] A. Voegelin, S. Pfister, A.C. Scheinost, M. Marcus, R. Kretzschmar, Changes in zinc speciation in field soil after contamination with zinc oxide, Environmental Science and Technology 39 (2005) 6616–6623.

[54] H. Bode, K. Dehmelt, J. Witte, Zur Kenntnis der Nickelhydroxidelektrode-I. Über das Nickel (II)-Hydroxidehydrat, Electrochimica Acta 11 (1966) 1079–1087.

[55] A.N. Mansour, C.A. Melendres, Analysis of X-ray absorption spectra of some nickel oxycompounds using theoretical standards, Journal of Physical Chemistry A 102 (1998) 65–81.

[56] J.W. Lukens, J.J. Bucher, D.K. Shuh, N.M. Edelstein, Evolution of technetium speciation in reducing grout, Environmental Science and Technology 39 (2005) 8064–8070.

[57] A.R. Halbert, K.A. Gebauer, L.M. Wall, Prognosis of occupational chromate dermatitis, Contact Dermatitis 27 (1992) 214–219.

[58] Y.L. Guo, B.J. Wang, K.C. Yek, J.C. Wang, H.H. Kao, M.T. Wang, H.C. Shih, C.J. Chen, Dermatoses in cement workers in Southern Taiwan, Contact Dermatitis 40 (1999) 1–7.

[59] J. Geier, A. Schnuch, A comparison of contact allergies among construction and non-construction workers attending contact dermatitis clinics in Germany. Results of the IVDK from November 1989 until July 1993, American Journal of Contact Dermatitis 6 (1995) 86–94.

[60] M.L. Peterson, G.E. Brown Jr., G.A. Parks, C.L. Stein, Differential redox and sorption of Cr(III/VI) on natural silicate and oxide minerals: EXAFS and XANES results, Geochimica et Cosmochimica Acta 61 (16) (1997) 3399–3412.

[61] C.A. Johnson, F.P. Glasser, Hydrotalcite-like minerals $(M_2Al(OH)_6(CO_3)_{0.5} \cdot XH_2O$, where $M = Mg$, Zn, Co, Ni) in the environment: synthesis, characterization and thermodynamic stability, Clays and Clay Minerals 51 (2003) 1–8.

[62] R. Dähn, A.M. Scheidegger, A. Manceau, M.L. Schlegel, B. Baeyens, M.H. Bradbury, M. Morales, Neoformation of Ni phyllosilicate upon Ni uptake on montmorillonite: a kinetics study by powder and polarized extended X-ray absorption fine structure spectroscopy, Geochimica et Cosmochimica Acta 66 (13) (2002) 2335–2347.